Spin relaxation in CdTe quantum dots with a single Mn atom

Marko D. Petrović and Nenad Vukmirović*
Scientific Computing Laboratory, Institute of Physics Belgrade, University of Belgrade, Pregrevica 118, 11080 Belgrade, Serbia
(Received 7 February 2012; published 9 May 2012)

We investigate spin relaxation times in CdTe quantum dots doped with a single Mn atom, a prototype of a system where the interaction between a single charge carrier and a single spin takes place. The theoretical model used includes the electron-Mn spin exchange interaction responsible for mixing of the states of different spin in the basic Hamiltonian and electron-phonon interaction as a perturbation responsible for transitions between the states. It is found that the dominant electron-phonon interaction mechanism responsible for spin relaxation is the interaction with acoustic phonons through deformation potential. Electron and Mn spin relaxation times at room temperature take values in the range from microseconds at a magnetic field of 0.5 T down to nanoseconds at a magnetic field of 10 T and become three orders of magnitude larger at cryogenic temperatures. It is found that electron spin-orbit interaction has a negligible effect on spin relaxation times, while changes in the position of the Mn atom within the dot and in the dot dimensions can change the spin relaxation times by up to one order of magnitude.

DOI: 10.1103/PhysRevB.85.195311 PACS number(s): 72.25.Rb, 73.21.La, 71.70.Ej, 72.10.Di

I. INTRODUCTION

The potential of utilizing the spin degree of freedom as a classical bit in spintronic devices[1–3] and as a quantum bit in potential quantum information processing devices[4] has been largely recognized in the last two decades. Operation of these devices crucially depends on the ability to manipulate the spin degrees of freedom of the system.[5] However, in all realistic open systems, undesirable spin flips occur due to the interaction with the environment. It is therefore of great importance to understand and be able to quantitatively describe the mechanisms of spin dephasing and spin relaxation.

Physical systems which are expected to be particularly suitable for aforementioned applications are based on architectures that contain quantum dots—artificial nanostructures where charge carriers are confined in all three spatial directions.[6,7] Due to the quantum confinement effect, the spectrum of electronic states in quantum dots is discrete, and as a consequence, the phase space for relaxation and dephasing processes is greatly reduced.[8] Therefore, long spin lifetimes of electrons confined in quantum dots are expected.

In addition, quantum dots provide a playground where one can study fundamental interactions on a single carrier or spin level. Such a level of understanding is necessary before one can proceed to understand more complicated device structures. Quantum dots doped with a single Mn atom have drawn particular attention for fundamental studies in recent years. The manganese atom acts effectively as an additional spin 5/2 degree of freedom and therefore enables fundamental studies of interaction between a single charge and a single spin in these dots. The experimentally observed signature of this interaction is the splitting of an exciton line in the quantum dot photoluminescence spectrum.[9–13] Predictions that it is possible to optically manipulate the state of a Mn spin in the quantum dot[12,14,15] were recently realized in several experiments.[16–18]

However, very little is known about the lifetimes of Mn and electron spin in these dots. A theoretical analysis[19] of optical orientation experiments[17] provided estimates of hole and electron spin relaxation times necessary for Mn spin orientation to occur. In a very recent work, Mn spin relaxation times in quantum dots in the presence of a hole or an exciton were calculated based on a microscopic theory.[20] Other theoretical studies of quantum dots with Mn atoms[21–34] were focused on electronic, optical, magnetic, or transport properties without any discussion of spin lifetimes. Numerous studies of spin relaxation in quantum dots were restricted to quantum dots without a Mn atom[35–45] or to diluted magnetic semiconductor quantum dots with many Mn atoms.[46]

In this work, we calculate the relaxation times of Mn and electron spin caused by interaction with phonons in a singly negatively charged CdTe quantum dot containing one Mn atom. Our calculation is based on a microscopic theory that links the system geometry with spin relaxation times. In Sec. II we introduce the theoretical model used to describe the system at hand and relevant spin relaxation times. In Sec. III we present the results and analyze the effects of different electron-phonon interaction mechanisms, spin-orbit (SO) interaction, magnetic field, temperature, quantum dot dimensions, and Mn atom position. In Sec. IV we compare our results to theoretical results for spin relaxation in somewhat similar systems and experiments and analyze the strength of other possible spin relaxation mechanisms not included in our model.

II. THEORETICAL MODEL

In this section, we describe a theoretical model used to describe a CdTe quantum dot that contains one extra electron and one Mn atom placed in its interior. Such a scenario is experimentally realized in a layer of self-assembled quantum dots grown at a relatively low dot density such that interdot interactions are negligible.

The Hamiltonian of the system reads

$$\hat{H}_o = \hat{H}_{\text{el}} + \hat{H}_{\text{m-el}} + \hat{H}_B, \tag{1}$$

where $\hat{H}_{\text{el}}$ is the electronic Hamiltonian, $\hat{H}_{\text{m-el}}$ describes the interaction of the electron with the Mn spin, and $\hat{H}_B$ is the Zeeman term that describes the interaction of the electron and Mn spin with the external magnetic field. This Hamiltonian acts in the Hilbert space of the system, which is given as the direct product of the electron orbital space, electron spin space, and Mn spin space.

The first, electronic term reads

$$\hat{H}_{\text{el}} = \sum_{i,\sigma} E_{i,\sigma} \hat{c}^{\dagger}_{i,\sigma} \hat{c}_{i,\sigma}, \tag{2}$$

with $\hat{c}^{\dagger}_{i,\sigma}$ and $\hat{c}_{i,\sigma}$ representing electron creation and annihilation operators. Typical self-assembled quantum dots are much larger in the lateral plane (xy plane) than in the growth (z) direction, while they can take various shapes—lenses, pyramids, truncated pyramids, etc. For this reason, we adopt the simplest possible quantum dot model that captures all essential features of the single-particle electronic spectrum—a rectangular box with in-plane dimensions (L_x and L_y) much larger than the dimension in the z direction (L_z) with infinite potential barriers outside of the region $0 \leqslant x \leqslant L_x$, $0 \leqslant y \leqslant L_y$, $0 \leqslant z \leqslant L_z$. The electronic states in the conduction band of semiconductor nanostructures within the first several hundreds of milli–electron volts are well described with the envelope function effective mass Hamiltonian. For our quantum dot model, the conduction band electron envelope function is then given as

$$\psi(x,y,z) = N_c \sin\left(\frac{n_x \pi}{L_x} x\right) \sin\left(\frac{n_y \pi}{L_y} y\right) \sin\left(\frac{n_z \pi}{L_z} z\right), \tag{3}$$

where $N_c = \sqrt{8/(L_x L_y L_z)}$ is the normalization constant and n_x, n_y, and n_z are positive integers that represent orbital quantum numbers in each direction. The single-particle energy $E_{i,\sigma}$ of an electronic state i with orbital quantum numbers n_x, n_y, and n_z is given as

$$E_{i,\sigma} = \frac{\hbar^2 \pi^2}{2m^*}\left(\frac{n_x^2}{L_x^2} + \frac{n_y^2}{L_y^2} + \frac{n_z^2}{L_z^2}\right), \tag{4}$$

where m^* is the effective mass of the conduction band electron in CdTe.

The second term $\hat{H}_{\text{m-el}}$ describes the exchange interaction between an electron and a Mn atom, and it is given by the spin impurity model Hamiltonian,[47] a model well established in previous theoretical studies of CdTe quantum dots with a few Mn atoms:[21,23–25,30,31]

$$\hat{H}_{\text{m-el}} = -\frac{1}{2}\sum_{i,j} J_{ij}(\mathbf{R})[(\hat{c}^{\dagger}_{i,\uparrow}\hat{c}_{j,\uparrow} - \hat{c}^{\dagger}_{i,\downarrow}\hat{c}_{j,\downarrow})\hat{M}_z + \hat{c}^{\dagger}_{i,\downarrow}\hat{c}_{j,\uparrow}\hat{M}^{+} + \hat{c}^{\dagger}_{i,\uparrow}\hat{c}_{j,\downarrow}\hat{M}^{-}]. \tag{5}$$

In Eq. (5), $\mathbf{R}$ is the position of the Mn atom and $J_{ij}(\mathbf{R})$ is the electron-Mn spin coupling strength, equal to $J_c \psi_i^*(\mathbf{R})\psi_j(\mathbf{R})$. $\hat{M}_z$, $\hat{M}^+$, and $\hat{M}^-$ are the Mn spin operators, whose properties are governed by the spin 5/2 algebra.

The last term of $\hat{H}_o$, also known as the Zeeman term, describes the interaction of the whole system with an external magnetic field B parallel to the z direction. It is given as

$$\hat{H}_B = -\mu_B g_e B \hat{S}_z - \mu_B g_{Mn} B \hat{M}_z, \tag{6}$$

where μ_B is the Bohr magneton, and g_e (g_{Mn}) is the electron spin (Mn spin) g factor. $\hat{S}_z$ is the operator of the z component of the electron spin.

In Sec. III C, we also consider electronic SO coupling that arises in materials lacking inversion symmetry (Dresselhaus SO coupling):[48]

$$\hat{H}_{\text{so}} = \gamma \mathbf{h} \cdot \sigma, \tag{7}$$

where σ-s are Pauli matrices, $\mathbf{h}$ is the Dresselhaus effective magnetic field,

$$\mathbf{h} = \left[k_x\left(k_y^2 - k_z^2\right), k_y\left(k_z^2 - k_x^2\right), k_z\left(k_x^2 - k_y^2\right)\right], \tag{8}$$

with $\mathbf{k} = -i\nabla$, and γ is the Dresselhaus SO coupling strength.

After numerically solving the Hamiltonian eigenvalue problem, we obtain the eigenenergies E_a and eigenstates $|\Psi_a\rangle$

$$\hat{H}_o|\Psi_a\rangle = E_a|\Psi_a\rangle, \quad |\Psi_a\rangle = \sum_{i,S_z,M_z} c^a_{iS_zM_z}|i,S_z,M_z\rangle. \tag{9}$$

We use i and S_z to denote the orbital and spin state of the electron and M_z for the Mn spin state.

Electron-phonon interaction is considered to be the main mechanism responsible for the transitions between the eigenstates $|\Psi_a\rangle$ and, consequently, spin relaxation. We show in Sec. III A that relevant transition energies are of the order of meV, which are typical energies of acoustic phonons. Because of the high energy of optical phonons compared to acoustic ones, we consider only the interaction with acoustic phonons. The Hamiltonian of electron-phonon interaction is given as[7,47]

$$\hat{H}_{\text{e-ph}} = \sum_{\mathbf{q},\lambda,ij} M_{\mathbf{q},\lambda} F_{ij}(\mathbf{q})(\hat{c}^{\dagger}_{i,\uparrow}\hat{c}_{j,\uparrow} + \hat{c}^{\dagger}_{i,\downarrow}\hat{c}_{j,\downarrow})(\hat{b}^{\dagger}_{\mathbf{q},\lambda} + \hat{b}_{-\mathbf{q},\lambda}) \tag{10}$$

where $\hat{b}^{\dagger}$ and $\hat{b}$ are phonon creation and annihilation operators and $\mathbf{q}$ is the phonon wave vector. For acoustic phonons, a linear dispersion relation connects the phonon wave vector and its energy $\omega = qv$, where v is the sound velocity for a particular acoustic phonon branch in a given material. $F_{ij}(\mathbf{q})$ is the electron-phonon interaction form factor, given as $F_{ij}(\mathbf{q}) = \int \psi_i^*(\mathbf{r}) e^{i\mathbf{qr}} \psi_j(\mathbf{r}) \mathrm{d}^3\mathbf{r}$.

The scattering matrix $M_{\mathbf{q},\lambda}$ depends on the type of electron-phonon interaction. For the interaction through the deformation potential, it is given as[47]

$$|M_{\mathbf{q},\lambda}|^2 = \frac{\hbar D^2 |\mathbf{q}|}{2V\rho v_{\text{LA}}}, \tag{11}$$

and for the interaction through the piezoelectric field it can be represented as[47]

$$|M_{\mathbf{q},\lambda}|^2 = \frac{\hbar \xi}{v_{\text{LA}}} \frac{(3q_x q_y q_z)^2}{|\mathbf{q}|^7} \tag{12}$$

for longitudinal phonons and

$$|M_{\mathbf{q},\lambda}|^2 = \frac{\hbar \xi}{v_{\text{TA}}}\left[\frac{q_x^2 q_y^2 + q_y^2 q_z^2 + q_z^2 q_x^2}{|\mathbf{q}|^5} - \frac{(3q_x q_y q_z)^2}{|\mathbf{q}|^7}\right] \tag{13}$$

for transversal ones. For transversal acoustic (TA) phonons there are two branches ($\lambda = 2, 3$), whereas for longitudinal acoustic (LA) phonons there is only one branch ($\lambda = 1$). In the preceding expressions D is the acoustic deformation potential, ρ is the CdTe material mass density, V is the volume of the system, and ξ is given as

$$\xi = \frac{32\pi^2 e^2 h_{14}^2}{\kappa V \rho},$$

where κ is the static dielectric constant and h_{14} is the piezoelectric constant.

For the work presented here, we have used the following parameters: $J_c = 15$ eV Å^3, $m^* = 0.106\, m_0$,[23] $g_e = -1.67$, $g_{Mn} = 2.02$,[25] $\gamma = 11.74$ eV Å^3,[49] $v_{LA} = 3083$ m/s, $v_{TA} = 1847$ m/s, $h_{14} = 3.94 \times 10^8$ V/m,[46] $D = 5.1$ eV, $\rho = 4.85 \times 10^3$ kg/m^3, and $\kappa = 9.6$.[50] Unless otherwise stated, quantum dot dimensions were taken as $L_x = 150$ Å, $L_y = 140$ Å, $L_z = 30$ Å. In our calculations, we consider first $N = 10$ electron orbitals, which gives the Hilbert space of $N_{max} = 120$ basis vectors. This ensures that the calculated quantities have converged to their real values.

Because of the fact that the electron–acoustic phonon interaction term is much smaller compared to the rest of the Hamiltonian, this term can be treated as a perturbation responsible for transitions between eigenstates $|\Psi_a\rangle$ of $\hat{H}_o$. If the system starts in an initial state $|\Psi_i\rangle$, it will make a transition to a final state $|\Psi_f\rangle$ due to electron-phonon scattering. The scattering rate for this process is determined by Fermi's golden rule:

$$\Gamma_{if} = \frac{2\pi}{\hbar} \sum_{\mathbf{q},\lambda} |M_{\mathbf{q},\lambda}|^2 |\langle \Psi_f | e^{i\mathbf{qr}} | \Psi_i \rangle|^2 \times \left(\bar{n}_{\mathbf{q},\lambda} + \frac{1}{2} \pm \frac{1}{2} \right) \delta(E_f - E_i \pm \hbar\omega_{\mathbf{q},\lambda}), \quad (14)$$

where E_i and E_f are the energies of the unperturbed system in the initial and the final state, $\bar{n}_{\mathbf{q},\lambda}$ is the mean number of phonons at a given temperature, and $|\langle \Psi_f | e^{i\mathbf{qr}} | \Psi_i \rangle|$ is the form factor for electron-phonon interaction. The plus sign in Eq. (14) corresponds to the process of phonon emission, while the minus sign corresponds to phonon absorption.

We show in Sec. III that most of the eigenstates of $\hat{H}_o$ have a well-defined Mn and electron spin because one of the $c_{iS_zM_z}$ coefficients in Eq. (9) is typically significantly larger than the others. Nevertheless, the remaining coefficients, which correspond to basis states with other values of S_z and M_z, are nonzero. For this reason, the transitions between states with different values of electron (or Mn) spin are allowed despite the fact that the electron-phonon interaction Hamiltonian is spin independent.

To obtain the average electron spin relaxation time one has to consider all possible transitions in the system where a particular change of spin occurs. For example, the mean relaxation time for electron spin change from the initial spin $S_z = 1/2$ to the final spin $S_z = -1/2$ is given as

$$\frac{1}{\tau} = \frac{\sum_i f_i \sum_f \Gamma_{if}}{\sum_i f_i}, \quad (15)$$

where the sum over i includes all possible initial states with $S_z = 1/2$ and the sum over f includes all possible final states with $S_z = -1/2$, with f_i being the thermal weighting factor of state i at a temperature T, given as $f_i = \exp[-E_i/(k_B T)]$.

III. RESULTS

A. Energy spectrum

The energy spectrum of CdTe quantum dots with a single Mn atom has been studied in the past,[21,30,51] and here we only review the main features, with an emphasis on those that are relevant for our work. Relevant energies for our problem are the single-particle electron orbital energies $E_{i,\sigma}$ [Eq. (4)], the

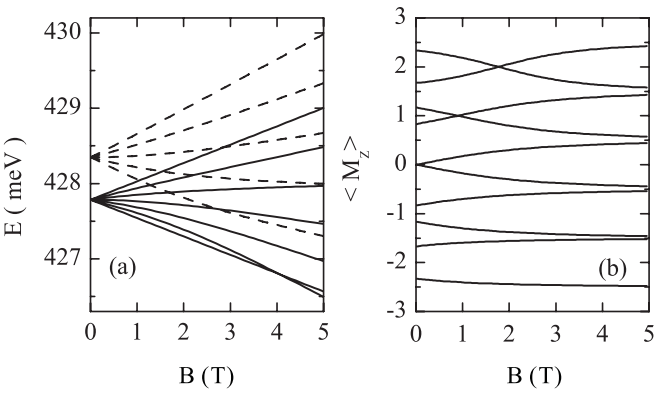

FIG. 1. Magnetic field dependence of (a) the energies of the first 12 energy levels produced by Zeeman splitting and electron-Mn exchange interaction and (b) the expected value of the Mn spin along the direction of an applied magnetic field. The system is considered without SO interaction and the Mn atom is placed at $\mathbf{R} = (7.4, 6.9, 1.6)$ nm.

electron-Mn spin exchange interaction energy $J_{ij}(\mathbf{R})$ [Eq. (5)], and the Zeeman splitting energy $\mu_B B$ [Eq. (6)]. The separation between the first two orbital energies is of the order of 50 meV and is much larger than the exchange interaction and Zeeman splitting energy, which are of the order of milli–electron volts. As a consequence, the first 12 eigenstates of our system all originate from the ground orbital state and are well separated from higher excited states, whose average populations are much smaller even at room temperature. The dependence of their energies on magnetic field is shown in Fig. 1(a).

Looking at the structure of energy levels for the electron–Mn atom system in Fig. 1(a), several distinctive features can be noticed. The spin of an electron is 1/2 and that of a Mn atom is 5/2. Combined, they will give two possible total spin numbers, $F = 2$ and $F = 3$, respectively, with five and seven spin projections along the direction of the external magnetic field. When there is no magnetic field, the total spin is a good quantum number and the presence of electron-Mn exchange interaction leads to a splitting of the12-fold degenerate ground level into two new, 7-fold and 5-fold degenerate ones. In the case of a finite magnetic field B, only F_z remains a good quantum number. The Zeeman term in the Hamiltonian eliminates all degeneracies, and 12 separate nondegenerate levels emerge.

A typical state of this system is a superposition of all basis vectors with the same total spin projection number F_z. Because electron-Mn spin coupling is relatively weak, there are only a few dominant states in this linear combination. The eigenstate wave function $|\Psi\rangle$ can be represented as

$$|\Psi\rangle = \alpha|0, +, M_-\rangle + \beta|0, -, M_+\rangle + \ldots, \quad (16)$$

where the basis vectors are ordered by the strength of their contribution to the eigenstate. In Eq. (16), $|0\rangle$ denotes the ground orbital state, $|+\rangle$ and $|-\rangle$ are the electron spin-up and spin-down states, while the Mn spin quantum number is related to F_z via $M_\pm = F_z \pm 1/2$, where $F_z = -2, \ldots, 2$. The next term in Eq. (16) depends mostly on the Mn-electron coupling strength $J_{0j}(\mathbf{R})$, i.e., on the position of the Mn atom.

For the study of Mn (and electron) spin relaxation, the next property that we should turn our attention to is the expected value of the Mn spin projection, M_z. Its dependence on the magnetic field for the first 10 levels with $F_z = -2, \ldots, 2$ is presented in Fig. 1(b). For most values of the magnetic field the expected values of M_z are very close to the corresponding half-integer values from the interval $-5/2$ to $5/2$, suggesting that Mn spin is well defined for a given eigenstate. This corresponds to the case where one of the α and β coefficients in Eq. (16) is much larger than the other. In such a case, the electron spin projection $S_z = F_z - M_z$ is also well defined. M_z and S_z cease to be well defined only for certain fields and for some states where energy level crossings occur (see Fig. 1). Spin relaxation times calculated within our approach should be taken with caution in such cases.

B. Spin relaxation time

Since the electron-phonon interaction Hamiltonian is independent of electron and Mn spin, phonons can only induce transitions between energy levels with the same total spin projection number. Under these conditions, there are only five downhill (as well as five uphill) transitions allowed. Each of these downhill transitions corresponds to Mn spin-flip from $M_z = F_z + 1/2$ to $M_z = F_z - 1/2$ and, at the same time, to electron spin-flop from $S_z = -1/2$ to $S_z = 1/2$.

The transition time between the two states with the same F_z is therefore also the relaxation time for Mn spin-flip from $M_z = F_z + 1/2$ to $M_z = F_z - 1/2$. On the other hand, to obtain the electron spin relaxation time, one has to take the average over all possible transitions that lead to an electron spin-flip or spin-flop.

The dependence of Mn and electron spin relaxation times on the magnetic field in the case of a Mn atom placed near the center of the dot [at $\mathbf{R} = (7.4,6.9,1.6)$ nm] at room temperature is shown in Figs. 2(a) and 2(b).

The external field affects the degree of Zeeman splitting, which, as a consequence, determines the energy of the phonon through which the system can relax. Since a linear dispersion relation connects the phonon energy and its wave vector, the external field impact on spin relaxation times comes mostly from scattering matrix elements [defined in Eqs. (11)–(13)]. For relaxation through the deformation potential, the scattering matrix element is $\sim$q, while for the piezo field it is $\sim 1/q$. Along with the q^2 factor that comes from the integration over $\mathbf{q}$ in Eq. (14), this gives an overall $\sim 1/q^3$ dependence for relaxation time through deformation potential and $\sim 1/q$ dependence for the relaxation time through the piezo field. As a consequence, spin relaxation becomes more probable as the external field increases, as shown Fig. 2(a). The above-mentioned $\sim 1/q^3$ and $\sim 1/q$ dependences are only approximately followed because the form factor [Eq. (14)] also depends on $\mathbf{q}$, but this dependence is relatively weak in the range of magnetic fields of our interest.

Figure 2(a) shows that the results for all possible transitions are very similar, ranging from microseconds to nanoseconds when the magnetic field varies. This comes from the fact that phonon energies for each transition are very similar. At zero magnetic field, the total spin $\mathbf{F}$ (in addition to F_z) becomes a good quantum number. Due to independence

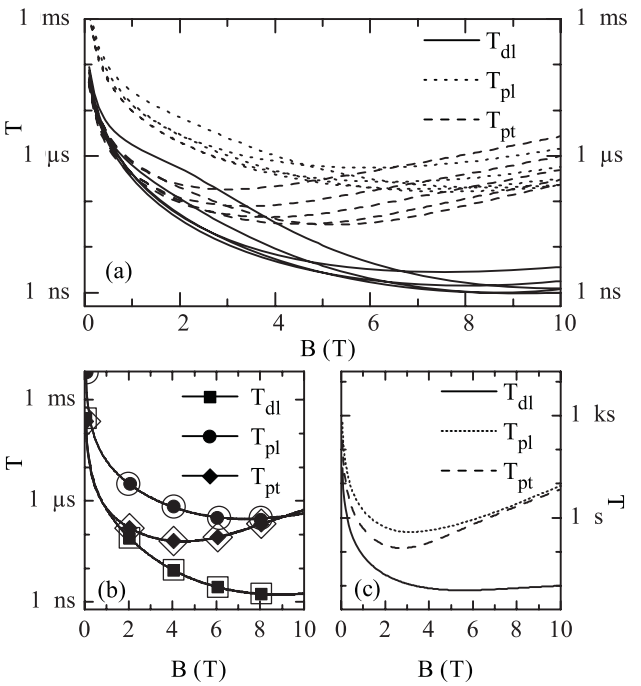

FIG. 2. Spin relaxation times for a Mn atom placed at $\mathbf{R} = (7.4,6.9,1.6)$ nm at room temperature ($T = 295$ K), caused by deformation potential interaction with LA phonons (dl) and piezoelectric potential interaction with LA phonons (pl) and TA phonons (pt). (a) Five transitions corresponding to Mn atom spin-flip. (b) Electron spin relaxation time obtained by averaging. Open symbols represent the data for the spin-down to spin-up process, while filled symbols represent the opposite. (c) The same as (b) but for the calculation performed using an inaccurate approximation.

of the electron-phonon interaction Hamiltonian on spin, the transitions between states with either different F or different F_z become forbidden. This leads to infinite relaxation times at $B = 0$ in our model.

Besides the Mn spin, the electron spin relaxation also occurs. As mentioned above, a consequence of the spin conserving Hamiltonian is the connection between these two. Each time a Mn atom makes a *flip* to a neighboring spin state, the electron makes a *flop*, and therefore the electron spin relaxation time is obtained by averaging over all possible transitions. The similarity between these two can be seen in Fig. 2(b). There are two types of processes for electrons: from spin-down to spin-up state and the opposite. In general there is a difference between the relaxation times for these two but only in the case of sufficiently low temperatures.

As mentioned earlier, one or, at most, two coefficients in Eq. (16) give the dominant contribution to an eigenstate. Both of these coefficients correspond to the ground orbital state. It is therefore very tempting to introduce an approximation in which we would reduce the Hilbert space of the system to basis states that originate from the orbital ground state only. However, this is not appropriate since such an approximation would yield infinite relaxation times. A less drastic approximation, where the eigenstates are calculated accurately, but only the first two terms in Eq. (16) are kept for the calculation of transition rates, is also highly inaccurate. As shown in Fig. 2(c), it gives unrealistically large spin relaxation times. The results

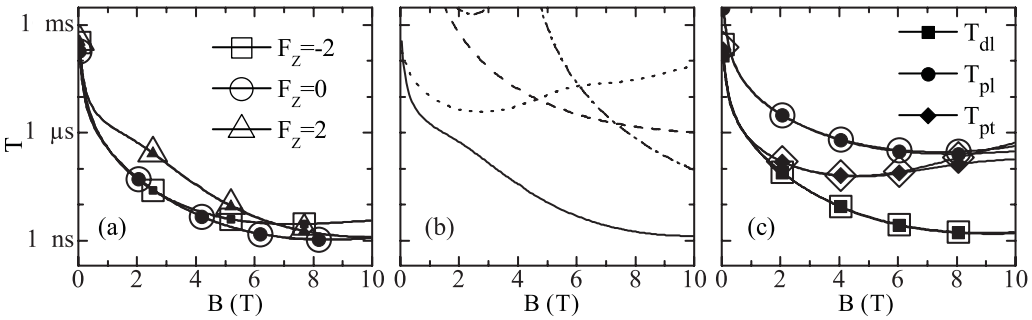

FIG. 3. Influence of Dresselhaus SO interaction on spin relaxation times for a Mn atom placed at $\mathbf{R} = (7.4,6.9,1.6)$ nm. Magnetic field dependence of relaxation time caused by the deformation potential interaction with LA phonons for (a) the transition between two levels with the same mean value of F_z in the presence (filled symbols) and absence (open symbols) of SO interaction and (b) the transitions between the level ($F = 3$, $F_z = 2$) and other levels. The solid line represents data for the transition to ($F = 2$, $F_z = 2$), while the dashed, dotted, and dash-dotted lines correspond to transitions to ($F = 3$, $F_z = 1$), ($F = 2$, $F_z = 1$), and ($F = 3$, $F_z = 3$) respectively. Transitions to other levels that are not shown have relaxation times longer than 1 ms. Levels were labeled according to the quantum numbers F and F_z, which are good quantum numbers at zero magnetic field in the absence of SO interaction. (c) Magnetic field dependence of average electron spin-up to spin-down relaxation time in the presence (filled symbols) and absence (open symbols) of SO interaction. dl, pl, and pt have the same meaning as in Fig. 2.

obtained from these tempting, but inaccurate, approximations demonstrate the necessity of including a larger number of orbital states in the calculation and the need for a numerical, rather than an analytical, approach to the problem.

C. The role of SO interaction

The electron (Mn) spin relaxation processes caused by spin-independent electron-phonon interaction are only possible due to the presence of terms in $\hat{H}_o$ that mix the states of different spins. Such a term in $\hat{H}_o$ is the electron-Mn exchange interaction $\hat{H}_{\text{m-el}}$, which mixes both states of different electron spin and states of different Mn spin.

Another term which leads to mixing of states of opposite electron spin is the SO interaction [Eq. (7)]. The results presented in Sec. III B were obtained while neglecting this term and the goal here is to assess the accuracy of such an approximation.

In the presence of SO interaction, F_z is no longer a good quantum number. However, it turns out that the mean value of F_z for an eigenstate is very close to the value of F_z in the absence of SO interaction. Therefore, the eigenstates of the Hamiltonian can still be labeled by the mean value of F_z for a state.

In Figs. 3(a) and 3(c) we compare the electron spin relaxation times in the presence and absence of Dresselhaus SO interaction. The values appear to be rather similar, which suggests a weak effect of Dresselhaus SO interaction on spin relaxation times.

A qualitative difference that the Dresselhaus SO interaction introduces is that it allows for transitions between states with different values of F_z, since F_z is no longer a good quantum number. Calculated transition rates for such transitions from the lowest state, with $F_z = 2$, to other states are shown in Fig. 3(b). These transitions appear to be much weaker than the transitions between states with the same F_z.

As a conclusion to this section, we may say that the changes in spin relaxation times due to Dresselhaus SO interaction are very small, and for all practical purposes, the Dresselhaus SO interaction can be neglected. Therefore, the rest of the results presented in this paper do not include SO interaction.

These results may appear rather surprising given that the Dresselhaus SO coupling parameter γ is comparable to the electron-Mn exchange coupling parameter J_c. However, one should note that Dresselhaus SO coupling couples only the states that originate from different orbital states. This claim is valid for our quantum dot model and any other quantum dot model that exhibits $x \to -x$, $y \to -y$, and $z \to -z$ symmetries. Since the energetic separation between such states is much larger than the coupling parameter, the Dresselhaus SO coupling therefore causes only weak mixing between states of different spin. On the other hand, the electron-Mn exchange coupling parameter mixes states that originate from the same orbital states. The corresponding coupling constant is comparable to the energy level separation between such states and, consequently, causes stronger mixing between states of different spin. This in turn leads to higher spin relaxation rates in the system.

D. Mn position and temperature

The position of the Mn atom determines the electron-Mn exchange coupling strength $J_{ij}(\mathbf{R})$ [Eq. (5)], which is the only place where it appears in the Hamiltonian. Since this is the only term in the Hamiltonian that mixes the states of different electron or Mn spin, one may expect that it has a significant effect on spin relaxation times. To understand the role of the Mn atom position on spin relaxation times, we have performed a calculation for two positions of Mn atom. Position 1 is near the center of the dot at $\mathbf{R} = (7.4,6.9,1.6)$ nm, while position 2 was chosen to maximize the $J_{01}(\mathbf{R})$ coupling strength and is given as $\mathbf{R} = (4.5,7,1.5)$ nm. The obtained spin relaxation times are shown in Fig. 4. At position 1, the J_{01}, J_{02}, and J_{03} coupling parameters are nearly zero. As a consequence, the states of interest have the first largest contribution in the linear combination [Eq. (16)] other than α and β from coefficients corresponding to orbital state $|4\rangle$ [$c^a_{4S_zM_z}$ coefficients in the notation of Eq. (9)]. On the other hand, at position 2, the first largest contribution other than α and β comes from $c^a_{1S_zM_z}$.

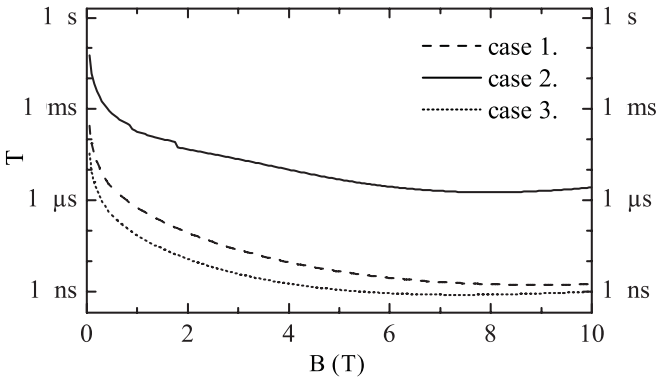

FIG. 4. Influence of Mn atom position and temperature on electron spin relaxation times. Dependence of the spin relaxation time for the transition from $S_z = 1/2$ to $S_z = -1/2$ on the magnetic field for different temperatures T and Mn ion positions $\mathbf{R}$: case 1—$T = 295$ K, $\mathbf{R} = (7.4,6.9,1.6)$ nm; case 2—$T = 3$ K, $\mathbf{R} = (7.4,6.9,1.6)$ nm; case 3—$T = 295$ K, $\mathbf{R} = (4.5,7.0,1.5)$ nm.

Since state $|1\rangle$ has a lower energy than state $|4\rangle$, the coefficients $c^a_{1S_zM_z}$ for position 2 are larger than $c^a_{4S_zM_z}$ coefficients in the case of position 1. As a consequence, the relevant states at position 2 exhibit a stronger mixing of basis states of different spin, which translates into faster spin relaxation at position 2, as shown in Fig. 4.

Spin relaxation times at temperatures of 3 and 295 K are also shown in Fig. 4. When an individual transition is concerned, the temperature appears in our theory only through the phonon occupation number, and consequently, its effect is easily predictable—higher temperatures lead to shorter spin relaxation times. When average spin relaxation times are involved, the temperature appears in the theory also through the thermal weighting factors [Eq. (15)]. This becomes especially important at higher magnetic fields, where the state with $F_z = 3$ becomes the ground state. The transition probability from this state to other states is small but this state has a high weighting factor. The average transition rate is then significantly different from the transition rate for individual transitions between states with the same F_z ($F_z = -2, \ldots, 2$). As a consequence of all the mentioned temperature effects, cooling down the system from room temperature to cryogenic temperature leads to an increase in spin relaxation times by three orders of magnitude.

E. Quantum dot dimensions

The dependence of spin relaxation times on quantum dot dimension L_z is shown in Fig. 5(a). The relative position of an Mn atom inside the dot is kept during this change of dimensions. The electron orbital states [Eq. (3)] in the range of energies that is of interest here all have quantum number $n_z = 1$. As a consequence, their energies do not change when L_z is changed (up to an irrelevant constant). Therefore, the change in L_z affects only the electron wave functions and, consequently, the electron-Mn exchange coupling parameters $J_{ij}(\mathbf{R})$. When the dot dimensions and the confinement volume increases, the probability of finding an electron near the Mn atom, due to normalization of the wave function, decreases. As a consequence, $J_{ij}(\mathbf{R})$ parameters decrease. This leads

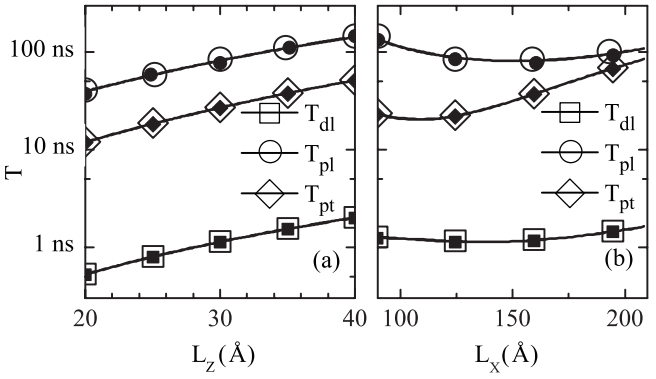

FIG. 5. Influence of quantum dot dimensions on electron spin relaxation times at a temperature of $T = 295$ K and magnetic field of $B = 5$ T. Filled symbols represent data for the spin-up to spin-down process, while open symbols represent the opposite. dl, pl, and pt have the same meaning as in Fig. 2. The Mn atom is placed at $\mathbf{R} = (4.5,7.0,1.5)$ nm for the default dot dimensions and its relative position is kept constant when dot dimensions are varied. (a) Dependence of the electron spin relaxation time on the dot dimension in the z direction. (b) Dependence of the electron spin relaxation time on the dot size in the xy plane: the L_x/L_y ratio and L_z are kept constant, while L_x is varied.

to weaker mixing of states of different spin, and therefore spin relaxation times increase when quantum dot dimensions increase, as shown in Fig. 5(a).

For the same reasons [weaker $J_{ij}(\mathbf{R})$ for larger dots], one may expect that the relaxation times will increase when the dot dimensions in the xy plane increase. However, the trend obtained in Fig. 5(b) is somewhat different. The reason is that when L_x and L_y increase, the distance between electron orbital energies [Eq. (4)] decreases. This leads to stronger contributions from basis states that originate from electron orbital states other than $|0\rangle$ [the missing terms in Eq. (16)], i.e., to stronger mixing of states of different spin in the expansion from Eq. (16), which leads to shorter spin relaxation times. To summarize, an increase in dot dimensions in the xy plane leads to a decrease in $J_{ij}(\mathbf{R})$ and to an increase in mixing in Eq. (16). As a consequence of these two opposite trends, one obtains a nonmonotonous dependence of spin relaxation times on L_x.

IV. DISCUSSION

In this section, we discuss the relevance of other possible spin relaxation mechanisms which were not included in our model and compare our results to other relevant results from the literature. In this work, we have so far only considered Dresselhaus SO coupling, which is a consequence of bulk inversion asymmetry. Realistic quantum dots also exhibit Rashba SO coupling[52] as a consequence of structural inversion asymmetry. Our model quantum dot is symmetric, therefore Rashba SO coupling is not present. However, realistic quantum dots certainly exhibit a certain degree of asymmetry and, consequently, Rashba SO coupling. The interplay of Dresselhaus and Rashba SO coupling in quantum dots was studied in Ref. 42. It was found that both of these are of similar strength and cause similar spin relaxation times. Moreover, in Ref. 35 the authors found that Dresselhaus SO

coupling provides a bigger admixture of states of different spin. Since we have found that Dresselhaus SO coupling has practically no effect on spin relaxation rates in our system, it is expected that the same will be the case for Rashba SO coupling. Nevertheless, to be certain of such a conclusion, we have performed additional calculations where the Rashba SO interaction of the form $\hat{H}_R = \gamma_R(\sigma_x k_y - \sigma_y k_x)$ was included. The realistic value of $\gamma_R = 1$ meV Å was taken.[42] We have performed the calculations (a) with both the Rashba and the Dreselhauss SO interaction included and (b) with only Rashba SO interaction included. In both cases it was found that inclusion of the SO interaction yields a negligible influence on spin relaxation times.

Spin relaxation by direct electron spin-phonon coupling in GaAs quantum dots was also considered in Refs. 35,53. The conclusion was reached that it is by far less effective than the relaxation caused by SO-interaction-induced mixing and electron-phonon interaction.

Spin relaxation due to hyperfine interaction between the electron spin and the spin of the nuclei was investigated in Ref. 36. The hyperfine interaction was found to be the dominant mechanism responsible for spin relaxation rates at magnetic fields which are low enough. Since our model gives relaxation rates that tend to zero at vanishing magnetic field, one may expect that hyperfine interaction will become relevant at low magnetic fields in our system too.

Direct coupling of Mn spin to phonons was considered in Ref. 20 as a potential mechanism of Mn spin relaxation. The corresponding relaxation times were found to be at least of the order of 1 ms, much longer than the ones originating from other mechanisms in our work.

Based on the discussion above, we may say that the spin relaxation mechanism considered in our work is certainly the most relevant mechanism in the system studied.

Next, we compare the trends that we obtain for the dependence of relaxation times on various parameters to those obtained in quantum dots without Mn atoms. In Ref. 39, spin relaxation in GaAs quantum dots caused by the presence of SO interaction and electron-acoustic phonon interaction was investigated. In that situation, spin relaxation takes place due to the transition between the first two Zeeman sublevels of opposite spin. The only spin mixing mechanism in such a system is the SO interaction. Spin relaxation times were found to decrease with the increase in magnetic field and were found to be mainly determined by the value of the phonon wave vector responsible for the transition. These conclusions, as one might have expected, are the same in our work. Interestingly, it was found in Ref. 39, on the other hand, that the dominant electron-phonon interaction mechanism that causes spin relaxation is piezoelectric interaction with TA phonons. In our system, the piezoelectric interaction with TA phonons is comparable to the deformation potential interaction with LA phonons at low magnetic fields, whereas at higher magnetic fields the deformation potential interaction with LA phonons becomes the dominant relaxation mechanism. Where the dependence of relaxation times on dot dimensions in the xy plane is concerned, it was found in Ref. 39 that these decrease when dot dimensions increase. The presence of exchange interaction between the electron and the Mn spin, as the dominant spin mixing mechanism in our system, causes a different trend in our case, as shown in Sec. III E. It was found that spin relaxation times increase with the increase in dot dimensions in the z direction both in our work and in Ref. 39, albeit for a different reason. In our case, this is caused by the decrease in electron-Mn spin exchange coupling strength when the dot volume increases (see Sec. III D), while in Ref. 39 this is caused by the decrease in SO interaction.

Finally, we compare the electron spin relaxation times that we obtained to the limits on their values inferred from Mn spin optical orientation experiments.[17] In Ref. 19, a theoretical analysis of Mn spin optical orientation experiments[17] was performed to understand the physical origin of the observed Mn spin orientation. It was found that optical orientation that occurs on the ∼10-ns time scale[17] can be explained if hole spin relaxation times of the order of ∼10 ns are assumed. Similar hole spin relaxation times were obtained from a microscopic theory in Ref. 20. At the same time, the electron spin relaxation time needs to be longer than that.[19] Our theoretical results at a low temperature and low magnetic field ($B < 1$ T) (Fig. 4) indicate electron spin relaxation times longer than tens of microseconds, which is fully consistent with the conclusion obtained in Ref. 19.

V. CONCLUSION

In conclusion, we found that the interactions responsible for electron and Mn spin relaxation in quantum dots doped with a single Mn atom are the electron-Mn spin exchange interaction and the electron-phonon interaction. The former provides mixing of the states with different spin within an eigenstate and allows for the spin-flip transition caused by the latter. SO interaction has a negligible effect on spin relaxation times, in contrast to conventional quantum dots, where SO interaction is the only mechanism which allows for mixing of states of different spin within an eigenstate and the relaxation through the interaction with phonons. Among the different electron-phonon interaction mechanisms, deformation potential interaction with LA phonons turns out to be the dominant mechanism responsible for spin relaxation. Spin relaxation times decrease with the increase in magnetic field. This dependence is mainly determined by an increase in energy level splitting and, consequently, the increase in the wave vector of the phonon responsible for the transition. The position of the Mn ion within the dot determines the strength of the electron-Mn spin exchange interaction and therefore significantly alters the spin relaxation times. We find that spin relaxation times in our electron-Mn spin system are longer than in similar hole-Mn spin or exciton-Mn spin systems. This suggests that potential spintronic or quantum computing devices based on the interaction between charge carriers and Mn spin should use electrons as charge carriers.

ACKNOWLEDGMENTS

This work was supported by a European Community FP7 Marie Curie Career Integration Grant (ELECTROMAT), the Serbian Ministry of Science (Project ON171017), and FP7 projects PRACE-1IP, PRACE-2IP, HP-SEE, and EGI-InSPIRE.

*Corresponding author: nenad.vukmirovic@ipb.ac.rs

[1] I. Žutić, J. Fabian, and S. Das Sarma, Rev. Mod. Phys. **76**, 323 (2004).

[2] M. W. Wu, J. H. Jiang, and M. Q. Weng, Phys. Rep. **63**, 61 (2010).

[3] K. A. van Hoogdalem and D. Loss, Phys. Rev. B **84**, 024402 (2011).

[4] D. D. Awschalom, D. Loss, and N. Samarth (eds.), *Semiconductor Spintronics and Quantum Computation* (Springer, New York, 2002).

[5] R. Heule, C. Bruder, D. Burgarth, and V. M. Stojanović, Phys. Rev. A **82**, 052333 (2010); Eur. Phys. J. D **63**, 41 (2011).

[6] D. Bimberg, M. Grundmann, and N. N. Ledentsov, *Quantum Dot Heterostructures* (John Wiley, Chichester, UK, 1999).

[7] P. Harrison, *Quantum Wells, Wires and Dots*, 2nd ed. (John Wiley and Sons, Chichester, UK, 2005).

[8] U. Bockelmann and G. Bastard, Phys. Rev. B **42**, 8947 (1990).

[9] L. Besombes, Y. Leger, L. Maingault, D. Ferrand, H. Mariette, and J. Cibert, Phys. Rev. Lett. **93**, 207403 (2004).

[10] Y. Leger, L. Besombes, L. Maingault, D. Ferrand, and H. Mariette, Phys. Rev. Lett. **95**, 047403 (2005).

[11] L. Besombes, Y. Leger, L. Maingault, D. Ferrand, H. Mariette, and J. Cibert, Phys. Rev. B **71**, 161307 (2005).

[12] J. Fernandez-Rossier, Phys. Rev. B **73**, 045301 (2006).

[13] A. K. Bhattacharjee and J. Pérez-Conde, Phys. Rev. B **68**, 045303 (2003).

[14] A. O. Govorov and A. V. Kalameitsev, Phys. Rev. B **71**, 035338 (2005).

[15] D. E. Reiter, T. Kuhn, and V. M. Axt, Phys. Rev. Lett. **102**, 177403 (2009).

[16] C. Le Gall, L. Besombes, H. Boukari, R. Kolodka, J. Cibert, and H. Mariette, Phys. Rev. Lett. **102**, 127402 (2009).

[17] C. Le Gall, R. S. Kolodka, C. L. Cao, H. Boukari, H. Mariette, J. Fernández-Rossier, and L. Besombes, Phys. Rev. B **81**, 245315 (2010).

[18] M. Goryca, T. Kazimierczuk, M. Nawrocki, A. Golnik, J. A. Gaj, P. Kossacki, P. Wojnar, and G. Karczewski, Phys. Rev. Lett. **103**, 087401 (2009).

[19] L. Cywiński, Phys. Rev. B **82**, 075321 (2010).

[20] C. L. Cao, L. Besombes, and J. Fernández-Rossier, Phys. Rev. B **84**, 205305 (2011).

[21] I. Savić and N. Vukmirović, Phys. Rev. B **76**, 245307 (2007).

[22] A. O. Govorov, C. R. Phys. **9**, 857 (2008).

[23] F. Qu and P. Hawrylak, Phys. Rev. Lett. **95**, 217206 (2005).

[24] F. Qu and P. Vasilopoulos, Phys. Rev. B **74**, 245308 (2006).

[25] F. Qu and P. Hawrylak, Phys. Rev. Lett. **96**, 157201 (2006).

[26] A. O. Govorov, Phys. Rev. B **72**, 075358 (2005).

[27] A. O. Govorov, Phys. Rev. B **72**, 075359 (2005).

[28] J. Fernandez-Rossier and L. Brey, Phys. Rev. Lett. **93**, 117201 (2004).

[29] J. Fernandez-Rossier and R. Aguado, Phys. Rev. Lett. **98**, 106805 (2007).

[30] N. T. T. Nguyen and F. M. Peeters, Phys. Rev. B **78**, 045321 (2008).

[31] N. T. T. Nguyen and F. M. Peeters, Phys. Rev. B **76**, 045315 (2007).

[32] N. T. T. Nguyen and F. M. Peeters, Phys. Rev. B **78**, 245311 (2008).

[33] N. T. T. Nguyen and F. M. Peeters, Phys. Rev. B **80**, 115335 (2009).

[34] E. Vernek, F. Qu, F. M. Souza, J. C. Egues, and E. V. Anda, Phys. Rev. B **83**, 205422 (2011).

[35] A. V. Khaetskii and Y. V. Nazarov, Phys. Rev. B **61**, 12639 (2000).

[36] S. I. Erlingsson and Y. V. Nazarov, Phys. Rev. B **66**, 155327 (2002).

[37] L. M. Woods, T. L. Reinecke, and Y. Lyanda-Geller, Phys. Rev. B **66**, 161318 (2002).

[38] E. Tsitsishvili, R. v. Baltz, and H. Kalt, Phys. Rev. B **67**, 205330 (2003).

[39] J. L. Cheng, M. W. Wu, and C. Lü, Phys. Rev. B **69**, 115318 (2004).

[40] L. M. Woods, T. L. Reinecke, and R. Kotlyar, Phys. Rev. B **69**, 125330 (2004).

[41] C. Lü, J. L. Cheng, and M. W. Wu, Phys. Rev. B **71**, 075308 (2005).

[42] D. V. Bulaev and D. Loss, Phys. Rev. B **71**, 205324 (2005).

[43] C. F. Destefani and S. E. Ulloa, Phys. Rev. B **72**, 115326 (2005).

[44] E. Tsitsishvili, R. v. Baltz, and H. Kalt, Phys. Rev. B **72**, 155333 (2005).

[45] O. Olendski and T. V. Shahbazyan, Phys. Rev. B **75**, 041306 (2007).

[46] W. Yang and K. Chang, Phys. Rev. B **72**, 075303 (2005).

[47] G. Mahan, *Many-Particle Physics* (Kluwer Academic, Dordrecht, 2000).

[48] G. Dresselhaus, Phys. Rev. **100**, 580 (1955).

[49] M. Cardona, N. E. Christensen, and G. Fasol, Phys. Rev. B **38**, 1806 (1988).

[50] K. H. Hellwege (eds.), *Numerical Data and Functional Relationship in Science and Technology, Landolt-Börnstein, New Series, Group III, Vol. 17, Part b* (Springer-Verlag, Berlin, 1982), pp. 113–149.

[51] S.-J. Cheng, Phys. Rev. B **72**, 235332 (2005).

[52] Y. L. Bychkov and E. I. Rashba, Phys. Rev. **39**, 78 (1984).

[53] A. V. Khaetskii and Y. V. Nazarov, Phys. Rev. B **64**, 125316 (2001).